The ultraviolet photochemistry of diacetylene: Direct detection of primary products of the metastable $C_4H_2^* + C_4H_2$ reaction

Ralph E. Bandy, Chitra Lakshminarayan, Rex K. Frost, and Timothy S. Zwier[a)]
Department of Chemistry, Purdue University, West Lafayette, Indiana 47907-1393

(Received 11 September 1992; accepted 15 December 1992)

The products of diacetylene's ultraviolet photochemistry over the 245–220 nm region are directly determined for the first time. At these wavelengths, the photochemistry is thought to proceed from a metastable excited state of C_4H_2 rather than by direct photolysis. The experimental method employs a small reaction tube attached to a pulsed nozzle. C_4H_2 is excited within the reaction tube where collisions of $C_4H_2^*$ with C_4H_2 form products which are subsequently ionized by vacuum ultraviolet radiation (118 nm) in the ion source of a time-of-flight mass spectrometer. The $C_4H_2^* + C_4H_2$ reaction produces C_6H_2 ($+C_2H_2$), C_8H_2 ($+2H,H_2$), and C_8H_3 ($+H$), all in good yield. An extensive set of experiments is carried out to ensure that the products observed are initial products formed by single-photon excitation of gas phase C_4H_2. Under certain conditions, secondary products formed by subsequent reaction of the initially formed products with C_4H_2 are also observed. These are dominated by $C_{10}H_3$ and $C_{12}H_3$. Thermochemical arguments are made which point to $C_8H_3+C_4H_2$ as the source of these secondary products. Collisional deactivation of $C_4H_2^*$ from its initially excited energy ($\sim$120 kcal/mol above the ground state) to the lower levels of the metastable state ($\sim$74 kcal/mol) is important in determining the relative amounts of C_8H_2 and C_8H_3 products. In cases where $C_4H_2^*$ undergoes extensive deactivation prior to reaction, C_8H_3+H products dominate. When collisional deactivation is minimized, much of the C_8H_3 products are formed with enough energy to subsequently dissociate further to form C_8H_2+2H. Mechanisms are postulated for the observed reactions and some suggestions for further work to assess the importance of these reactions in planetary atmospheres are given.

I. INTRODUCTION

Several of the planets and moons of our solar system are known to have hydrocarbons as significant constituents of their atmospheres.[1] Through a combination of solar irradiation and electron bombardment, these hydrocarbons are formed from methane via a complex network of reactions. Titan, a moon of Saturn, is perhaps the best breeding ground for larger hydrocarbons due to the low H_2 and high N_2 content of its atmosphere.[2,3] However, the atmospheres of Neptune,[4] Uranus,[5,6] Triton,[7] and to some extent Jupiter[8] and Saturn,[9] also all have significant methane photochemistry. Analysis of spectra from the Voyager missions has led to the unambiguous identification of diacetylene as a constituent of the atmosphere of Titan.[10] As a result, diacetylene is currently one of the most complex hydrocarbons confirmed to be present in planetary atmospheres outside our own.

Diacetylene is thought to play an important role in several aspects of the atmosphere's properties.[2] First, C_4H_2 is known to be photochemically very reactive, and hence capable of producing yet larger hydrocarbon molecules. Second, diacetylene's absorptions, which extend to longer wavelengths than those of acetylene, serve as a partial ultraviolet radiation shield for larger hydrocarbons once they are formed. As pointed out by Yung *et al.*,[2] C_2H_2 and C_4H_2 thus play roles somewhat analogous to that of ozone in earth's atmosphere. Third, the larger C_nH_2 polyynes, which are assumed to be the products of diacetylene photochemistry, have been proposed as a potential source of the visible absorptions in aerosol hazes present in the planetary atmospheres.[2–9] Fourth, current models predict that condensation of C_4H_2 and its photochemical products account for much of the loss of carbon from the gas phase.[2–9] Finally, the photochemical models[2] predict that C_4H_2 plays a significant role in removing hydrogen atoms from the atmospheres via recombination reactions which form H_2.

Diacetylene is also noteworthy for its role in soot formation, especially in acetylene flames.[11] Diacetylene has been shown to be a significant product in the pyrolysis and photochemistry of acetylene.[12,13] Rate constants for the pyrolytic loss of diacetylene as a function of temperature have also been determined,[12] but little is known about the nature of the pyrolysis products or the mechanisms of the pyrolysis reactions.

The gas phase photochemistry of C_4H_2 has been studied first in cursory fashion by Pontrelli[14] and later in more detail by Glicker and Okabe.[15] The latter authors determined a photochemical quantum yield for C_4H_2 loss of 2.0 ± 0.5 throughout the region from 255 to 144 nm. Yet, despite the large quantum yield for reaction, they were unable to detect any gas phase products at wavelengths longer than 200 nm, observing only the polymeric end product which formed on the walls of the reaction vessel. Glicker and Okabe presented convincing evidence that the photochemistry occurring at these wavelengths did not in-

a)Author to whom correspondence should be addressed.

 0021-9606/93/075362-13$06.00

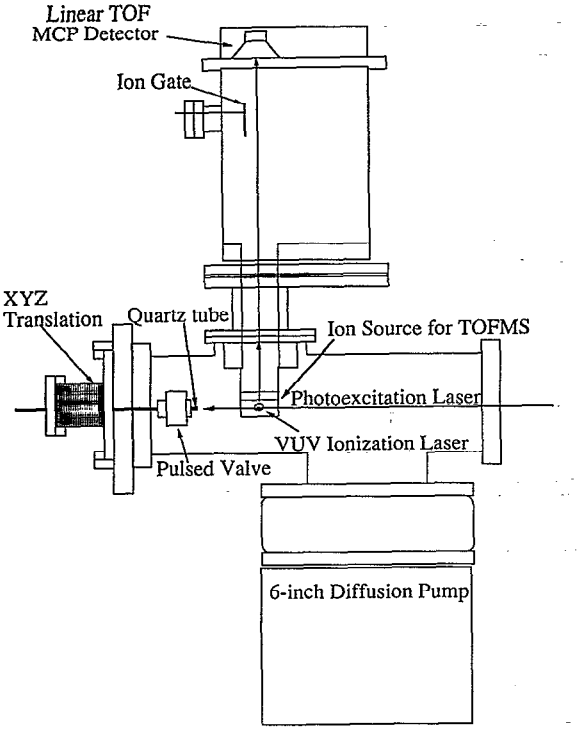

FIG. 1. A schematic of the instrument used to study the photochemistry of diacetylene. The photoexcitation laser is shown propogating down the axis of the quartz tube, though it was brought perpendicular to the tube in some experiments.

volve free radical intermediates. The excited state of C_4H_2 postulated to be responsible for its photochemistry is a metastable $^3\Delta_u$ state 3.2 eV above the ground state.[16]

Lacking direct experimental data, current photochemical models of the planetary atmospheres assume that C_8H_2 is the sole initial product of diacetylene photochemistry formed via the reaction

$$C_4H_2^* + C_4H_2 \rightarrow C_8H_2 + H_2 , \quad (1)$$

where $C_4H_2^*$ refers to a metastable state of diacetylene.[2–9]

We have recently reported briefly on photochemical studies which have directly detected the ultraviolet photochemical products of the $C_4H_2^* + C_4H_2$ reaction.[17] Here we present a full account of this work. This study builds directly on our previous spectroscopic study of the $^1\Delta_u \leftarrow {}^1\Sigma_g^+$ transition of diacetylene (over the wavelength region 217–245 nm) which used resonant two-photon ionization in a supersonic molecular beam.[18] The initial photochemical products of diacetylene include not only C_8H_2, but also $C_6H_2(+C_2H_2)$ and $C_8H_3(+H)$, all with good yield.

II. EXPERIMENT

Figure 1 shows a schematic of the instrument used to carry out the photochemical studies of diacetylene. The methods used to synthesize and handle diacetylene have been described previously.[18] A mixture of 1%–10% C_4H_2 in helium is introduced directly into the ion source region of the time-of-flight mass spectrometer through a Laser-technics pulsed valve operating at 20 Hz ($\sim$250 μs long). Photochemistry is initiated in a small quartz reaction tube attached to the end of the pulsed valve. C_4H_2 pulsed into this tube is excited to various vibronic levels of the $^1\Delta_u \leftarrow {}^1\Sigma_g$ transition using the doubled output of an excimer-pumped dye laser (0.1–0.5 mJ/pulse). Photochemical products travel 7 cm downstream, where they are ionized by 118 nm vacuum ultraviolet (VUV) light as they pass through the source region of the mass spectrometer, typically 60–80 μs after photoexcitation. The resulting ions are then mass analyzed in a linear time-of-flight mass spectrometer and detected using a microchannel plate ion detector.

A 1.0 μs long, 800 V pulse is applied to a plate in the flight tube to pulse away most of the $C_4H_2^+$ ions before they reach the microchannel plate (MCP) detector. This signal, roughly 1000 times larger than that of the products without ion gating, can saturate the MCP, interfering with the detection of the small product ion signals arriving at later times.

The photoexcitation laser wavelength is tuned over the range 245–217 nm, requiring the use of three different Coumarin dyes to span the entire wavelength region. The 118 nm VUV photons are produced by tripling the third harmonic (355 nm) output of a Nd:YAG laser in xenon gas.[19] These 118 nm (10.5 eV) photons provide a general and gentle ionization scheme for most hydrocarbon products of interest here since the photon energy exceeds the ionization potential[20] (I.P.) of C_4H_2 (10.18 eV) and that of its higher mass photoproducts. Mass spectra taken without the photoexcitation laser show no significant fragmentation of C_4H_2. The xenon gas cell used for tripling is 100 cm in length and 1.9 cm in diameter. The cell is equipped on the input side with a 50 cm f.l. quartz lens to focus the 355 nm light (10–15 mJ/pulse) into the Xe/Ar gas mixture. The output side has a LiF lens for transmission of the 118 nm light. Generation of 118 nm light is optimal for this cell using 16 Torr of Xe and 177 Torr of Ar. Both the 355 and 118 nm beams pass through the ion source. However, interference from the 355 nm light is negligible for two reasons. First, the wavelength dependence of the refractive indices of the lenses permits differential focusing of the 355 and 118 nm light in the source region. Second, spatial separation of the 355 and 118 nm laser beams is achieved by off-axis incidence of the 355 nm light on the input quartz lens. The VUV laser power has not been measured in our laboratory, but is expected to be about 100 nJ/pulse assuming a conversion efficiency for tripling in xenon of $\sim 1 \times 10^{-5}$ from earlier reports.[19]

Two features of the experimental method seem crucial to the successful observation of initial photochemical products in this system. First, the photochemical products were observed only after the pulsed valve was placed directly in the ion source region without skimming the expansion. In so doing, the efficiency of product detection is greatly increased. In addition, placing the pulsed valve directly in the ion source region allows us to counterpropogate the laser down the reaction tube without difficulty. The "cyl-

inder" of excited C_4H_2 molecules created in this way results in product detection over a much longer time window than is possible with a perpendicular photoexcitation scheme. The lack of differential pumping has the drawback of limiting the total gas load considerably. The typical operating pressure in the TOF chamber was 8×10^{-6} Torr at an estimated nozzle backing pressure of about 5 Torr.

Second, the short length (0.5–1.0 cm) of *S*1-UV quartz tube (2 mm i.d.) constrains the expansion of the gas mixture for a time long enough to allow $C_4H_2^*/C_4H_2$ collisions, but short enough that the initial photochemical products are detected. A simple estimate bears this out. From the total gas flow from the nozzle, we estimate that the helium and C_4H_2 pressures in the reaction tube under typical conditions are about 2 and 0.1 Torr, respectively. The product arrival time distribution indicates that the average $C_4H_2^*$ molecule spends about 10 μs in the reaction tube. We thus estimate that the laser-excited C_4H_2 molecules experience about 200 collisions with helium atoms and 20 collisions with other diacetylene molecules during their time in the reaction tube. These are conditions well suited to initial product detection.

Several types of spectra are reported in this work. Difference mass spectra which highlight the photochemical products are taken by recording mass spectra with and without the photoexcitation laser present, typically with other conditions optimized for product detection. Resonant two-photon ionization spectra of the C_4H_2 reactant molecules provide diacetylene's absorption spectrum in the region of interest. Action spectra are recorded by monitoring the product ion intensities as a function of photoexcitation laser wavelength, with the excitation/VUV laser timing maximized for observation of products. The arrival time distribution of the products is recorded by changing the delay of the VUV laser relative to the photoexcitation laser.

III. RESULTS AND ANALYSIS

A. A review of C_4H_2 spectroscopy

Resonant two-photon ionization spectra of the $^1\Delta_u \leftarrow {}^1\Sigma_g^+$ transition of C_4H_2, C_4HD, and C_4D_2 cooled in a supersonic molecular beam have been recorded previously by our group.[18] Only vibronically induced transitions are observed in the resonant two-photon ionization (R2PI) spectrum, shown in Fig. 2, which is dominated by the $2_0^n6_0^1$ progression. ν_2 is a symmetric C≡C stretching mode, while ν_6 is a degenerate C–H bending mode which vibronically induces the transition.[18] The interpretation of the spectrum is complicated by the presence of Renner–Teller and Herzberg–Teller coupling. Excited state dynamics in the $^1\Delta_u$ vibronic levels is evidenced by the significant breadth of the spectral features. The peak widths in C_4H_2 increase with increasing excess energy, changing from about 5 cm^{-1} full width at half-maximum (FWHM) at the 6_0^1 level to near 40 cm^{-1} at the $2_0^26_0^1$ level. The widths of the corresponding transitions in C_4H_2, C_4HD, and C_4D_2 generally decrease with increasing deuteration, indicating that H atom motion plays an important role in the broadening

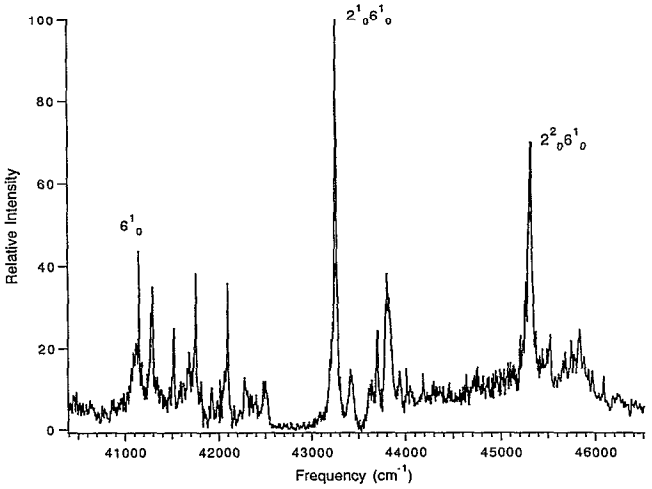

FIG. 2. Resonant two-photon ionization (R2PI) spectrum of the $^1\Delta_u \leftarrow {}^1\Sigma_g^+$ transition of C_4H_2 highlighting the $2_0^n6_0^1$ progression which is the main progression used to initiate photochemistry in the present study.

of the spectral features. State mixing of the $^1\Delta_u$ vibronic levels with a dense bath of background states, including that of the metastable $^3\Delta_u$ state, are believed to contribute to the observed broadening. Because of the dominance of the $2_0^n6_0^1$ progression, much of the photochemistry reported here is initiated by excitation of these transitions.

B. Difference mass spectra

Figure 3(a) shows a time-of-flight mass spectrum obtained by tuning the photoexcitation laser (PL) to 231.4 nm to excite the 2^16^1 vibrational level of the $^1\Delta_u$ state. Figure 3(b) shows a similar scan obtained without the PL. The difference spectrum in Fig. 3(c) clearly shows the photochemical products resulting from laser excitation of C_4H_2. The dominant peaks observed at mass 74, 98, and 99 correspond to the initial products C_6H_2, C_8H_2, and C_8H_3. Small amounts of $C_{10}H_3$ and $C_{12}H_3$ are also observed. The masses 86 and 88 seen in Figs. 3(a) and 3(b) are minor impurities from the synthesis of the diacetylene and have also been reported in the work of Glicker and Okabe.[15] The mass 78 impurity arises from residual benzene in the gas handling system from previous experiments carried out in our laboratory. The mass spectrum in Fig. 3(b) shows the presence of small amounts of C_6H_2 and C_8H_4 possibly formed due to thermal polymerization of diacetylene in the cylinder. By comparing the integrated ion intensity of $C_4H_2^+$ (without ion gating) to the photochemical product intensities, we estimate that the total product ion intensity is only about 0.2% of the diacetylene ion intensity under the present conditions.

It is unlikely that the observed product ion intensities are significantly affected by fragmentation during photoionization due to the gentle photoionization scheme employed. Less than 1% fragmentation of C_4H_2 is observed following VUV ionization. Given the similar nature of the photochemical products formed (especially C_6H_2 and

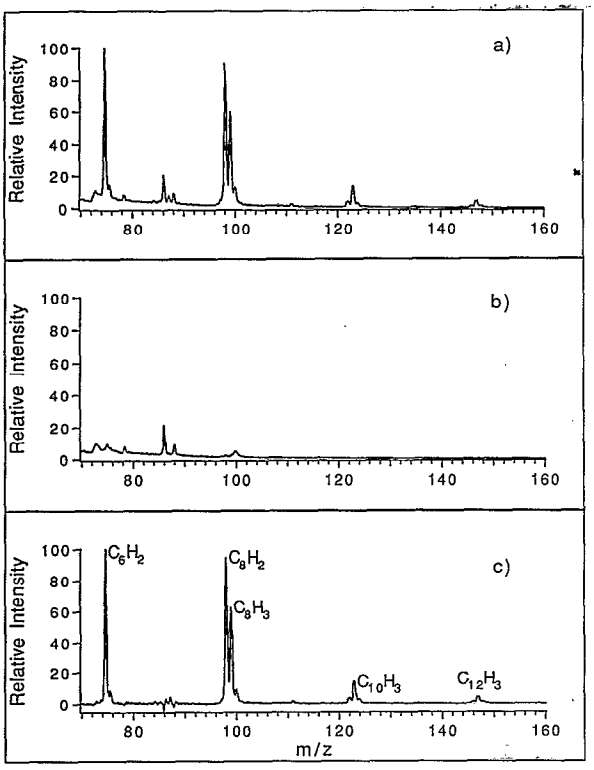

FIG. 3. Time-of-flight mass spectra (a) with the photoexcitation laser on; (b) with the photoexcitation laser off showing minor impurities present in the gas mixture; and (c) the difference mass spectrum highlighting the products of C_4H_2 photochemistry. The $C_4H_2^+$ ion arising from the C_4H_2 reactants (not shown) is 500 times the size of the product peaks shown.

C_6H_2), only minor fragmentation is expected in the product channels as well. In fact, previous work has established that the $C_nH_2^+$ ions have no open dissociation pathways within ~6 eV of their ionization thresholds.[21] Furthermore, the relative product intensities can be changed significantly with changing expansion conditions, pointing to the products arising from separate neutral product channels.

Evidence will be presented in succeeding paragraphs that C_6H_2, C_8H_2, and C_8H_3 are all primary products of the $C_4H_2^* + C_4H_2$ reaction. Some possible routes for forming these products from $C_4H_2 + C_4H_2^*$ are summarized in Table I along with estimates of the relevant reaction energies.[22] Reaction (5), which forms C_6H_3 (or C_6D_3 from the $C_4D_2^* + C_4D_2$ reaction), is not observed, though it is exothermic. We have been able to place an upper bound on the C_6H_3 (C_6D_3) intensity of 5% of that of C_6H_2 (C_6D_2). Based on Glicker and Okabe's work, the initial reactions proceed without the formation of free radical intermediates at the wavelengths of our study.[15] A schematic energy level diagram for the observed primary product channels is given in Fig. 4. The figure highlights the collisional deactivation of the excited C_4H_2 molecules which occurs concurrently with reaction. Table I thus gives limiting values of the reaction exothermicities proceeding from the laser-excited energy and from the fully deactivated $^3\Delta_u$ state of C_4H_2.[16] The observed product intensities thus will reflect the distribution of $C_4H_2^*$ energies present in the reaction mixture.

A small amount of signal is also present at mass 100. Much of this signal is due to the ^{13}C isotope of C_8H_3, but there are also indications that some of the intensity may be due to collisionally stabilized C_8H_4 reactant complex.

Table I also illustrates some possible routes for the formation of the secondary products formed by reaction of the initial products with additional C_4H_2 molecules. It is clear from Fig. 3(c) that these secondary products are dominated by $C_{10}H_3$ and $C_{12}H_3$. In fact, the $C_{10}H_2$, $C_{10}H_4$, $C_{12}H_2$, and $C_{12}H_4$ ion intensities are at least a factor of 5 less intense than $C_{10}H_3$ and $C_{12}H_3$ under all conditions we have studied. Based on the estimated reaction enthalpies of

TABLE I. C_4H_2 reaction thermochemistry.

Initial reactions	$\Delta H^0_{r\times n}$ (ground state)[a] (kcal/mol)	$\Delta H_{r\times n}$ (2^16^1)[b] (kcal/mol)	$\Delta H_{r\times n}$ $(^3\Delta_u)$[c] (kcal/mol)
(1) $C_4H_2 + C_4H_2^* \rightarrow C_8H_2 + H_2$	−3	−126	−77
(2) $C_4H_2 + C_4H_2^* \rightarrow C_6H_2 + C_2H_2$	0	−123	−74
(3) $C_4H_2 + C_4H_2^* \rightarrow C_8H_3 + H$	+60	−63	−14
(4) $C_4H_2 + C_4H_2^* \rightarrow C_8H_2 + 2\,H$	+101	−22	+27
(5) $C_4H_2 + C_4H_2^* \rightarrow C_6H_3 + C_2H$	+89	−34	+15
(6) $C_4H_2 + C_4H_2^* \rightarrow C_6H_2 + C_2H + H$	+130	+7	+56
Secondary reactions			
(7) $C_8H_3 + C_4H_2 \rightarrow C_{10}H_3 + C_2H_2$	~+1		
(8) $C_8H_3 + C_4H_2 \rightarrow C_{12}H_3 + H$	~−1		
(9) $C_8H_2 + C_4H_2 \rightarrow 2\,C_6H_2$	~−2		
(10) $C_6H_2 + C_4H_2 \rightarrow C_{10}H_2 + H_2$	~−1		
(11) $C_8H_2 + C_4H_2 \rightarrow C_{10}H_2 + C_2H_2$	~+2		
(12) $C_6H_2 + C_4H_2 \rightarrow C_{10}H_3 + H$	~+60		
(13) $C_8H_2 + C_4H_2 \rightarrow C_{12}H_3 + H$	~+60		

[a]Heat of reaction for ground state reactants.
[b]Heat of reaction for one C_4H_2 reactant excited to the 2^16^1 vibrational level of the $^1\Delta_u$ state. The $2^1_0\,6^1_0$ photon energy = 123.5 kcal/mol.
[c]Heat of reaction when one C_4H_2 molecule is excited to the $^3\Delta_u$ state. The 74 kcal/mol energy of the $^3\Delta_u$ state is taken from Ref. 16.

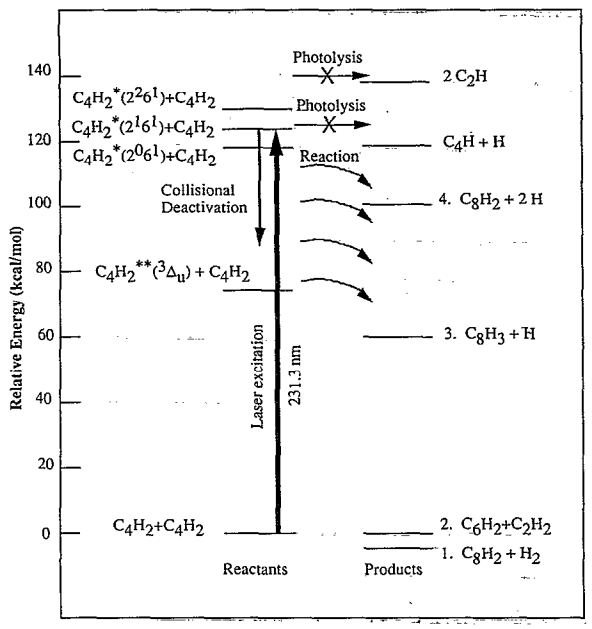

FIG. 4. A schematic energy level diagram of the ultraviolet photochemistry of diacetylene. The $^3\Delta_u$ state is a metastable excited state of C_4H_2. Reaction takes place from a distribution of energies determined by the extent of collisional deactivation of $C_4H_2^*$ toward the lower levels of the $^3\Delta_u$ state. The reaction enthalpies are estimates based on extrapolation of the heats of formation of C_2H_2, C_2H_3, and C_4H_2 from Ref. 22 to the larger C_nH_2 and C_nH_3 species.

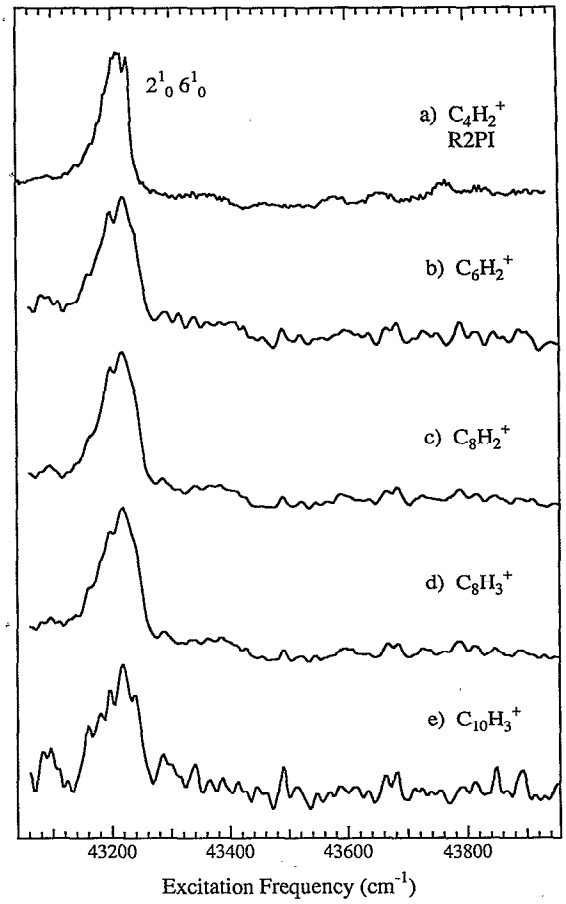

FIG. 5. (a) Resonant two-photon ionization scan in the $2^1_0 6^1_0$ region of the $^1\Delta_u \leftarrow {}^1\Sigma_g^+$ transition of gas phase C_4H_2 monitoring the $C_4H_2^+$ mass. (b)–(e) Action spectra of the photochemical products C_6H_2, C_8H_2, C_8H_3, and $C_{10}H_3$ in the $2^1_0 6^1_0$ region recorded with the photoexcitation and ionization lasers present.

Table I, the reactions of C_8H_3 with C_4H_2 [reactions (7) and (8)] are believed to be the major routes for formation of $C_{10}H_3$ and $C_{12}H_3$.

C. Action spectra

The action spectra of Fig. 5 confirm that the products observed are due to the gas phase photochemical reactions of C_4H_2. Figure 5(a) is a resonant two-photon ionization (R2PI) scan in the region of the $2^1_0 6^1_0$ transition of C_4H_2 recorded in the absence of the VUV laser. The C_4H_2 molecules are resonantly excited and ionized by two photons from the photoexcitation laser directly in the ion source region of the time-of-flight mass spectrometer (TOFMS). The breadth of the $2^1_0 6^1_0$ transition is significantly greater than that of Fig. 2 since the low nozzle backing pressures provide little cooling for the C_4H_2 in the present experiments. The action spectra seen in Figs. 5(b)–5(e) were obtained by tuning the photoexcitation laser while monitoring the product ions $C_6H_2^+$, $C_8H_2^+$, $C_8H_3^+$, and $C_{10}H_3^+$, respectively, created by VUV ionization. The faithful reproduction of the diacetylene absorption spectrum by the products prove that the products are being formed following photoexcitation of gas phase diacetylene. Similar action spectra of the products have been obtained over the 6^1_0 (243.1 nm) and the $2^2_0 6^1_0$ (220.7 nm) vibronic transitions of C_4H_2.

D. The energy dependence of product formation

Figures 6(a)–6(c) show mass spectra of the products obtained by tuning the photochemical laser to the 6^1_0 (243.1 nm), $2^1_0 6^1_0$ (231.4 nm), and $2^2_0 6^1_0$ (220.7 nm) vibronic features, respectively. The mass spectra show no differences which could be clearly attributed to energy-dependent effects on the product yields. The small differences which are observed in Fig. 6, especially those involving secondary products, are most likely caused by differences in laser power among the three scans.

The lack of a significant energy dependence to the product yields supports Glicker and Okabe's deduction that the photochemical reactions proceed from a metastable state of C_4H_2 rather than from free radical chemistry. Estimates of the C–H bond strength in C_4H_2 vary from 120–131 kcal/mol.[23] Even a 120 kcal/mol bond energy places the threshold for C_4H free radical formation at 235 nm, well above the energy of the 6^1 level. Thus, the observation of photoproducts following excitation at 243.1 nm and the lack of obvious differences between the product distributions over the 12 kcal/mol range investigated implies that the laser-excited vibronic levels of C_4H_2 are col-

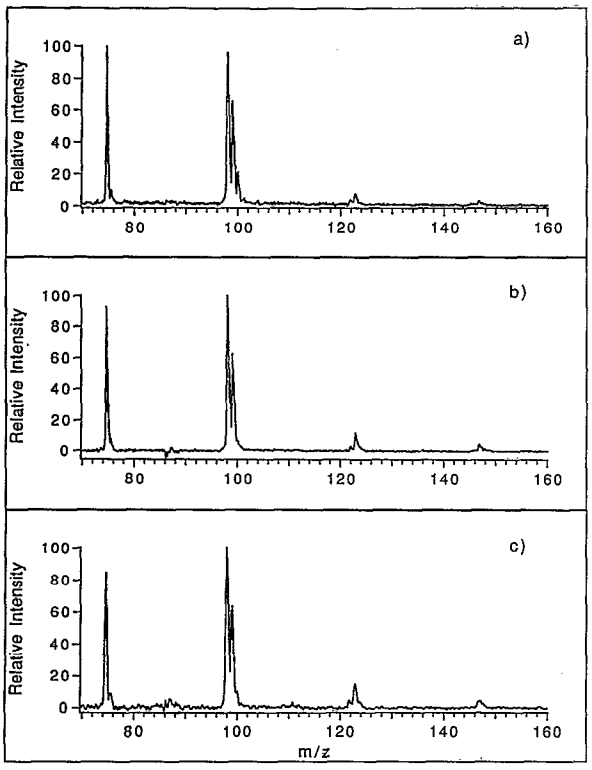

FIG. 6. Difference time-of-flight mass spectra of the photochemical products following excitation of C_4H_2 via the (a) 6_0^1; (b) $2_0^1 6_0^1$; and (c) $2_0^2 6_0^1$ vibronic transitions of the $^1\Delta_u \leftarrow {}^1\Sigma_g^+$ transition.

lisionally deactivated to a long lived metastable state which is itself capable of reaction with C_4H_2 without dissociation to C_4H+H.

Due to the lack of a significant energy dependence to the product yields, most of the studies outlined in the following sections excite C_4H_2 via the $2_0^1 6_0^1$ transition at 231.4 nm since it is the most intense feature in the absorption spectrum of diacetylene.

E. Photoexcitation laser power studies

Figure 7 shows the product signals (as a percentage of total product ion signal) for C_6H_2, C_8H_2, C_8H_3, $C_{10}H_3$, and $C_{12}H_3$ plotted as a function of the photoexcitation laser power when tuned to the $2_0^1 6_0^1$ transition. The weak dependence of the product percentages of C_6H_2, C_8H_2, and C_8H_3 on photoexcitation laser power indicates that the initial products are formed following absorption of a single photon by C_4H_2. A closer look at Fig. 7 reveals that there is a small increase in C_6H_2 percentage at the expense of C_8H_2 and C_8H_3 with increasing laser power. This small nonlinear component to the product signals likely results from thermal heating of the reaction mixture by the photoexcitation laser driving reactions which form C_6H_2. We estimate that the absorption of photons by diacetylene could give rise to a temperature rise in the helium-dominated mixture of as much as 50 K. Since reactions (7)–(10) in Table I are near thermoneutral, their rates may be significantly enhanced with increasing temperature.

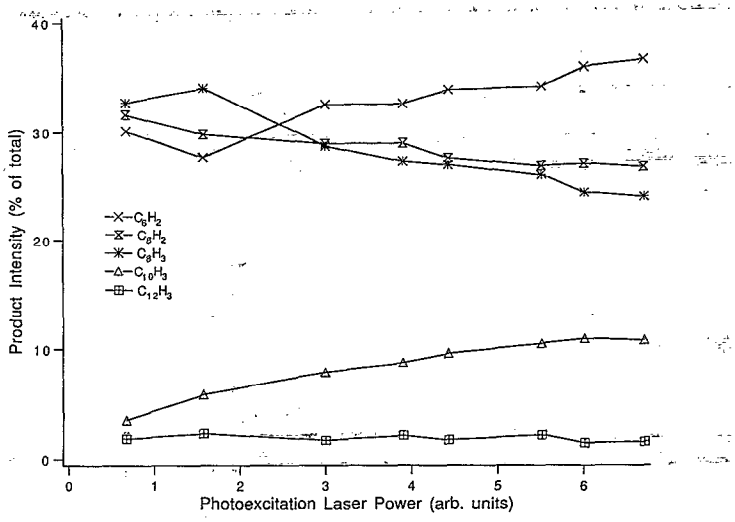

FIG. 7. Percentage of total product signal intensity plotted as a function of photoexcitation laser power. The reported percentages are integrated ion signals in a difference mass spectrum taken with the photoionization laser tuned to the peak arrival time for the products.

The stronger laser power dependence of the $C_{10}H_3$ signal shows clearly that its formation is enhanced by the additional energy deposited into the reaction mixture at high laser powers. Again, this excess energy may simply be required to raise the temperature of the gas mixture in order to drive near thermoneutral reactions such as

$$C_8H_3+C_4H_2 \rightarrow C_{10}H_3+C_2H_2 .$$

Alternatively, we cannot rule out the possibility that the $C_{10}H_3$ molecules are formed after absorption of a second photon by the initial products. The intensity of $C_{12}H_3$ product is too low to draw any clear conclusions regarding its power dependence.

F. Product arrival time distributions

Figure 8 shows scans of the intensity distributions of C_4H_2 and its photoproducts as a function of the time delay between the photoexcitation and ionization lasers. The photoexcitation laser counterpropagates the gas flow, exciting a cylinder of diacetylene molecules in the reaction tube which are subsequently swept into the ion source region. These scans thus map out the arrival time distribution of the products. The photoexcitation laser is fired as the peak of the gas pulse traverses the reaction tube, resulting in maxima in the product arrival times [Figs. 8(b)–8(e)] coinciding with the maximum in the $C_4H_2^+$ signal [Fig. 8(a)]. The delay of 65 μs between photoexcitation and photoionization lasers corresponds to an average product velocity of about 1×10^5 cm/s over 7 cm from the reaction tube to the center of the ion source. The width of the product peaks ($\sim$15 μs FWHM) reflects the time the excited volume of gas spends traversing the reaction tube before expanding into the chamber. Such short reaction times are important to the observation of primary, rather than secondary, $C_4H_2^* + C_4H_2$ products.

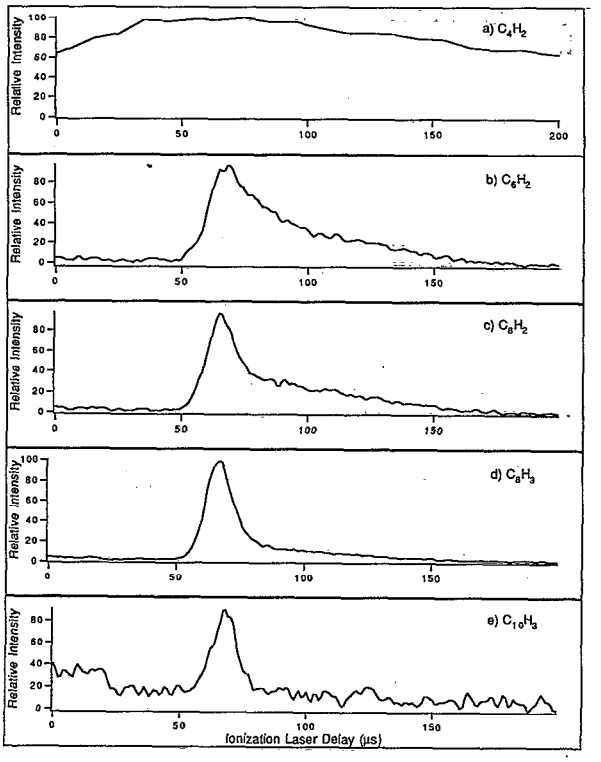

FIG. 8. (a) Reactant C_4H_2 concentration and (b)–(e) photoproduct signal intensity as a function of time delay between the photoexcitation and photoionization lasers. The maximum peak intensity is at 65 μs delay.

It is obvious from Fig. 8 that the arrival time distributions differ significantly from one product to the next. The C_8H_3 and $C_{10}H_3$ signals [Figs. 8(d) and 8(e)] are very sharply peaked about their maxima, while C_8H_2 [Fig. 8(c)] shows some tailing to longer arrival times which is further enhanced in C_6H_2 [Fig. 8(b)]. We have measured percent product intensities both as time-integrated signals and as single-time measurements at the maximum arrival time. The percent changes are not large ($<10\%$), but clearly favor C_6H_2 in the integrated mode.

There appear to be two contributing sources to the different arrival time distributions. First, even with the reaction tube present, the arrival time distributions of the products reflect to some extent both the kinematics and exothermicities of the reactions. As can be seen from Fig. 4, the C_8H_3+H product channel has the smallest reaction exothermicity and also produces a light hydrogen atom as C_8H_3's product partner. Both these features minimize the translational energy expected in the C_8H_3 product, narrowing its arrival time distribution. The channels producing C_8H_2 also produce either H_2 or 2H. Formation of the H_2 product results in a larger exothermicity, but with still poor kinematics for translational excitation in C_8H_2. The formation of C_8H_2+2H has little exothermicity and poor kinematics. Finally, the formation of C_6H_2 from a $C_4H_2^*$ + C_4H_2 collision complex is highly exothermic and requires the loss of a much heavier C_2H_2 fragment for its formation. The ejection of C_2H_2 should impart a higher recoil velocity to C_6H_2 resulting in a wider velocity distribution for these molecules which broadens their arrival time distribution.

We postulate that this effect may contribute not only to the broadening in the C_6H_2 arrival time about its maximum, but also to the long-time tail of the distribution. The C_6H_2 arrival time scan of Fig. 8(b) shows significant product signal even 50–100 μs after the peak arrival time. This is long enough that interactions with the walls of the reaction tube seem unavoidable. The larger translational velocity of the C_6H_2 products would render C_6H_2 more susceptible to reaching the walls before exiting the reaction tube. Once there, some adsorption to the walls may occur, followed by desorption later in the gas pulse, as observed. The contribution from the long-time tail in the C_6H_2 product channel also seems to be minimized when a new reaction tube is in place, pointing to a slow accumulation of C_6H_2 on the walls.

G. Wall effects

Action spectra of the photoproducts have established that the photochemical reaction products are formed following excitation of *gas phase* C_4H_2. However, the arrival time distributions of Sec. III F led us to consider the contribution from wall effects further. We have carried out difference mass spectra, arrival time scans, and action spectra using tubes of varying length and tube material. Both 5 and 10 mm long quartz tubes and a 10 mm long ceramic tube, all with a 2 mm inner diameter, have been used without significant change in the distribution of products. A ceramic disk was introduced in the nozzle face plate to eliminate all metal surfaces from the laser/reaction volume without effect. The contribution from thermal effects to product formation has also been tested by carrying out the study in a ceramic tube heated to 100 °C. Heating of the tube is achieved by wrapping nichrome wire around the tube which can be resistively heated. In the heated tube, no product formation has been observed in the absence of the photoexcitation laser. With the photoexcitation laser present, there is no change in the product state distribution relative to that in an unheated tube.

These studies indicate that the reaction tube fulfills its role of inducing collisions between the gas phase diacetylene molecules without significantly affecting the products observed. The great majority of the products appear not to experience a collision with the walls of the tube before exiting. The only observed effects of interactions with the walls involve the long arrival time tail on the C_6H_2 signal which is ascribed to adsorption/desorption of some C_6H_2 product molecules on the walls.

H. The role of collisional deactivation in the product distribution

As we have noted from the energy level scheme of Fig. 4, the extent of collisional deactivation of the excited state diacetylene molecules could play a significant role in the product yields observed. In order to understand these effects, we have carried out several studies aimed at varying

TABLE II. C_4H_2 flow study.[a]

Percent C_4H_2 in He	Relative product signal following VUV photoionization			
	C_6H_2	C_8H_2	C_8H_3	$C_{10}H_3$
2.5%	42%	31%	24%	2.0%
5.0%	44.5%	33%	21%	1.8%
7.5%	42%	35%	20%	3.0%
10%	41%	37%	19%	2.7%

[a]The flow study was carried out by varying the ratio of 10% C_4H_2 mixture and He while maintaining a total flow of 0.8 standard cm^3/min (sccm).

the extent of deactivation of $C_4H_2^*$ prior to reaction in order to view its effect on the product intensities.

1. C_4H_2 concentration studies

Concentration studies have been carried out in which the diacetylene concentration is varied over a factor of 4 (from 2.5% to 10% in helium) at a constant total reaction pressure. The low total flows necessitated by the present experimental arrangement hindered accurate control of flows (and hence of C_4H_2 concentration). Nevertheless, the results of this study, shown in Table II, show a clear trend in product intensities with increasing C_4H_2 concentration. While the percent signal due to C_6H_2 shows little change, there is a distinct tradeoff between the C_8H_2 and C_8H_3 percentages which favors C_8H_2 over C_8H_3 at higher C_4H_2 concentrations.

2. N_2 concentration studies

In most of our studies, helium has served as the buffer/diluent gas in our reaction mixtures. Diatomic nitrogen, with its vibration/rotation energy levels, will be significantly more efficient than helium in deactivating $C_4H_2^*$ to low energy levels of the metastable $^3\Delta_u$ state. Nitrogen is also the major constituent of Titan's atmosphere,[1,2] so that product intensities observed in nitrogen-dominated mixtures will more closely simulate a possible product distribution on Titan. To these ends, a series of difference mass spectra were taken with varying amounts of N_2 present in the expansion mixture. The flow of 5% C_4H_2/He is kept at a constant, low value throughout the series.

As seen in Fig. 9, the product state distribution changes dramatically with changes in nitrogen concentration. The relative amounts of C_6 and C_8 products are only weakly affected by N_2, with the percent C_6H_2 varying from 42% to 36% with increasing N_2. However, the C_8H_3/C_8H_2 intensity ratio varies by almost a factor of 10. Without N_2 present [Fig. 9(a)], the conditions of low C_4H_2 concentration result in the C_8H_n products being dominated by C_8H_2 with little C_8H_3 observed. By contrast, at high nitrogen concentrations [Fig. 9(c)], there is an intensity reversal between C_8H_2 and C_8H_3, so that C_8H_3 now dominates the product signals.

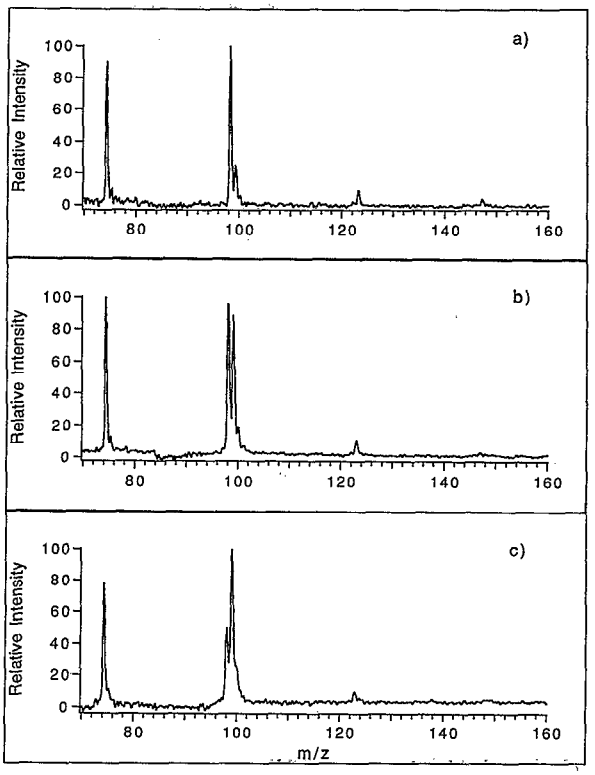

FIG. 9. Difference time-of-flight mass spectra of the photoproducts with 0.3 sccm C_4H_2/He mixture and (a) 0.0; (b) 0.6; and (c) 1.1 sccm N_2 in the expansion. Note the intensity transfer between C_8H_2 and C_8H_3 at high N_2 concentration.

3. Perpendicular excitation—varying the reaction time

The role of collisional deactivation in product state distribution is verified by studies in which the photoexcitation laser is crossed perpendicular to the quartz reaction tube. Excitation of the diacetylene mixture at various positions along the axis of the tube varies the time spent by $C_4H_2^*$ in the collision-dominated region within the reaction tube. Unfortunately, the perpendicular study necessitates focusing the photoexcitation laser onto the quartz tube to observe products. This results in an increase in the energy deposited in reaction mixture, which in turn drives secondary reactions of the type shown in Eqs. (7)–(10) in Table I. Despite this complication, the clear observation is that as the laser is brought closer and closer to the end of the tube (i.e., as the reaction time is shortened), the C_8H_3 product intensity drops relative to C_8H_2.

4. Explanation of the observed trends

The explanation of the above trends is found in the extent of deactivation of $C_4H_2^*$ in the mixture. As indicated in both Table I and Fig. 4, C_8H_2 can be formed from $C_4H_2^* + C_4H_2$ by two routes involving accompanied formation of either H_2 or two free hydrogen atoms. Since we do not directly detect either H_2 or H, we cannot directly distinguish these two routes. However, as Fig. 4 shows, the formation of two free hydrogen atoms can occur only from $C_4H_2^*$ molecules possessing at least 100 kcal/mol energy

above the ground state. Once deactivation to the lower levels of the $^3\Delta_u$ state has occurred, the C_8H_2+2H product channel is 27 kcal/mol endothermic (Table I). For a given C_4H_2 concentration, low N_2 flows result in inefficient deactivation of $C_4H_2^*$, so that a large fraction of $C_4H_2^*$ reacts from energies above the asymptote for formation of C_8H_2+2H. The C_8H_2+2H reaction channel likely proceeds by sequential loss of two hydrogen atoms, i.e.,

$$C_4H_2+C_4H_2^* \rightarrow C_8H_3^\ddagger+H, \quad (4a)$$

$$C_8H_3^\ddagger \rightarrow C_8H_2+H. \quad (4b)$$

As a result, inefficient deactivation of $C_4H_2^*$ favors formation of C_8H_2 at the expense of C_8H_3. As the N_2 pressure is raised, the $C_4H_2^*$ collisions with N_2 stabilize a larger and larger fraction of the $C_4H_2^*$ reactants below the threshold for formation of C_8H_2+2H. Then following loss of a hydrogen atom [reaction 4(a)], the $C_8H_3^\ddagger$ product has insufficient energy to lose a second hydrogen atom, resulting in a transfer of product intensity from C_8H_2 to C_8H_3 as observed. Note that even at the highest N_2 flows we have been able to explore, some C_8H_2 product remains [Fig. 9(c)]. This would suggest that at least some of the C_8H_2 product is formed with commensurate formation of H_2.

Similar arguments apply to the C_4H_2 concentration study. As the C_4H_2 concentration is raised in a C_4H_2/He mixture, the $C_4H_2^*$ molecules encounter and react with a C_4H_2 molecule following fewer and fewer deactivating collisions with helium. The result is that the C_8H_2/C_8H_3 intensity ratio increases with increasing C_4H_2, as is observed experimentally.

Finally, the shorter reaction times which accompany excitation near the end of the quartz tube also result in less collisional stabilization of $C_4H_2^*$ prior to exiting the reaction tube. The reactive collisions which do occur under these conditions are thus ones proceeding from a higher average internal energy in $C_4H_2^*$, resulting in an increase in the C_8H_2+2H channel relative to C_8H_3+H, as observed.

I. Photochemistry in isotopic mixtures of diacetylene

We have also studied isotopic mixtures containing C_4D_2, C_4HD, and C_4H_2 in order to determine what effect, if any, isotopic substitution has on the relative product intensities. Given the significant rearrangement of H/D atoms in the reactions (especially that accompanying $C_6H_2+C_2H_2$ formation), one might expect to see significant isotope effects. Furthermore, if it is possible to selectively excite one isotope in a mixture, the distribution of product isotopes would provide insight to the mechanisms of the reactions.

Starting with a mixture of C_4H_2, C_4HD, and C_4D_2 isotopes in the reaction mixture with the composition shown in Fig. 10(a), the R2PI spectra of each of the isotopes has been recorded in the $2_0^1 6_0^1$ spectral region. Our earlier study of the R2PI spectra of C_4H_2, C_4HD, and C_4D_2 (Ref. 18) indicated that in a cold molecular beam, isotopically selective excitation could be carried out. However, the low backing pressure ($\sim$5 Torr) used in the present experiments broadened the spectral transitions to the point that selective excitation is not possible.

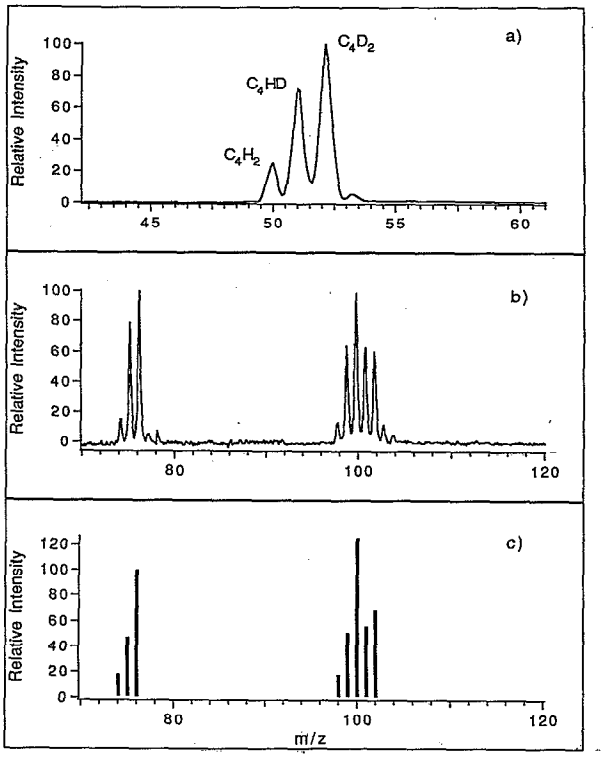

FIG. 10. (a) Time-of-flight mass spectrum of isotopes of diacetylene. (b) The difference time-of-flight mass spectrum of the photochemical products following excitation of the isotopic mixture in (a) to the $2^1 6^1$ level. (c) Product isotopic abundances expected following equal-efficiency excitation of the isotopic mixture in (a) followed by statistical dissociation of $(C_8H_nD_m)^*$ to the various isotopes of C_6H_2, C_8H_2, and C_8H_3 products.

Figure 10(b) shows the difference mass spectra obtained by excitation at a wavelength corresponding to the peak of the $2_0^1 6_0^1$ transitions of the isotopes. The mass spectra show a distribution of product isotopes which follow in a general way the reactant distribution of Fig. 10(a). One limiting case for the reaction mechanisms involves formation of a long-lived $(C_8H_nD_m)^*$ complex in which product formation occurs without any preference toward isotopic composition of the products. In this case, the relative intensities of the isotopes will be governed solely by the numbers of each type of $(C_8H_nD_m)^*$ complex formed with a statistical distribution of dissociation products of these complexes. Figure 10(c) plots the isotopic intensity distribution expected in this limiting case assuming equal excitation efficiencies for each isotope. The general agreement between experiment and calculation argues against any strong primary isotope effects in the reactions. The calculated distributions are skewed somewhat too heavily toward fully deuterated products. This may be a simple consequence of unequal excitation efficiencies of the isotopes. On the other hand, mechanisms which involve transfer of one H/D atom from each reactant molecule correct the distributions in the right direction. In the future, we hope to carry out the photochemistry under colder conditions in

which selective excitation of a single isotope can occur, since such experiments will provide much more information regarding the mechanisms of the reactions.

IV. DISCUSSION

The present results have shown that three primary products are formed from the $C_4H_2^*+C_4H_2$ reaction; namely, $C_6H_2+C_2H_2$, C_8H_2+2H/H_2, and C_8H_3+H. These products represent the first step in the ultraviolet photopolymerization of diacetylene vapor.[15] The observed C_6H_2 product we propose to be accompanied by formation of C_2H_2, though the C_2H_2 product is not directly observed in our study due to its high ionization potential. The formation of $C_6H_2+C_2H+H$ is not allowed on energetic grounds in the wavelength range we have studied (Table I).

The C_8H_3 product is intriguing because it provides an entry point to free radical processes even below the threshold for direct photolytic production of C_4H or C_2H free radicals from C_4H_2. As a free radical, C_8H_3 is anticipated to react readily with a wide range of hydrocarbons, including C_4H_2 itself. In fact, the detection of $C_{10}H_3$ and $C_{12}H_3$ as the dominant secondary products point to C_8H_3 as a likely source for their formation. The thermochemical estimates of Table I show the $C_8H_3+C_4H_2$ reactions forming $C_{10}H_3$ and $C_{12}H_3$ to be near thermoneutral. As a result, these may be able to proceed at a reasonable rate without absorption of another photon. Note that the $C_{10}H_2$ and $C_{12}H_2$ secondary products are about a factor of 5 less intense (Fig. 3), though the thermochemistry of their formation from $C_8H_2+C_4H_2$ is similar (Table I). The long conjugation length of C_8H_3 also points to it having ultraviolet absorptions which will likely produce photochemically active states. To the authors' knowledge, the spectroscopy of C_8H_3 is completely unexplored.

A. Thoughts on the mechanisms of product formation

In this section, potential mechanisms for formation of the three initial products C_6H_2 $(+C_2H_2)$, C_8H_3 $(+H)$, and C_8H_2 $(+2H/H_2)$ are given. The results of Glicker and Okabe,[15] confirmed by our work, leave little doubt that reaction occurs under the collision-dominated conditions of our study from a metastable state of C_4H_2 rather than through free radicals formed by photodissociation. Glicker and Okabe postulate the $^3\Delta_u$ state as the metastable state of C_4H_2 responsible for the photochemistry. This state has been observed in the electron scattering experiments of Allan at 3.21 eV above the ground state.[16] In the linear configuration, the transition to the ground state is both electric dipole and spin forbidden. The metastable state survives hundreds of collisions with helium or N_2. Since this state plays such a crucial role in diacetylene's photochemistry, experiments aimed at determining the geometry and lifetime of this state are needed.

The *ab initio* calculations of Karpfen and Lischka[24] indicate that both components of the Renner–Teller split $^3\Delta_u$ state ($^3A_u+{}^3B_u$ in C_{2h}) are derived from an electron configuration which places the excited electron in a π^* orbital which is antibonding between triply bonded carbon atoms, but adds bonding character between the singly bonded carbons. The result is a cumulene-like excited state structure such as that shown below

$$\dot{C}=C=C=\dot{C}.$$

The minimum energy configurations calculated for the ^3A_u and ^3B_u states incorporate a nearly linear carbon framework with hydrogens bent in *trans* configurations. This state, then, serves as one of the reactants in the ultraviolet photochemistry of C_4H_2. Having said this, it is also possible that, by analogy to acetylene's vinylidene structure, the cumulene may in fact be able to undergo H-atom transfer along the carbon chain as well.[13,25]

The diradical character of the cumulene-like excited state suggests that attack of this species on C_4H_2 will occur from the radical centers. If such attack occurs at the terminal carbon atoms of ground state C_4H_2, as shown in Fig. 11(a) a $C_8H_4^*$ reaction complex will be formed which has two resonance structures. The symmetric resonance structure has radical centers adjacent to each of the central hydrogens. We postulate that this structure may play a central role to the formation of C_8H_2 and C_8H_3 products since ejection of one or both of the central hydrogen atoms can occur directly from this resonance structure, as shown. The prediction of this mechanism is that formation of C_8H_2 will occur with loss of one hydrogen atom from each of the reactant species. On the other hand, if H-atom transfer occurs in $C_4H_2^*$ prior to reaction, asymmetric losses may occur. Further work using isotopically selective excitation will be needed to distinguish between these possibilities.

The mechanism for formation of $C_6H_2+C_2H_2$ must be somewhat more involved, given the extensive rearrangement which must occur. Lacking further information, we assume that the reaction forms triacetylene, although one cannot completely rule out the possibility that a novel cyclized product such as tetradehydrobenzene may be formed. Figure 11(b) suggests a mechanism for triacetylene+acetylene formation. The mechanism involves attack by $C_4H_2^*$ on one of the interior carbon atoms of C_4H_2. Such an attack would lead to a second set of resonance structures pictured in Fig. 12(b). Again, the resonance structure to the right has the radical centers adjacent to the H and C_2H groups which need to be ejected. The fact that C_2H and H are on adjoining carbon atoms makes ejection of C_2H_2 at least plausible, but this mechanism will probably need to undergo refinement as more mechanistic data become available.

One of the intriguing features of our results which a successful mechanism must explain is that no significant C_6H_3 products are formed even though this reaction channel is lower in energy than the C_8H_2+2H channel which we clearly observe. The suggested mechanism provides little help in understanding why the C_6H_3 product is not observed. Clearly, further experiments are required to understand the mechanisms of these reactions in more detail.

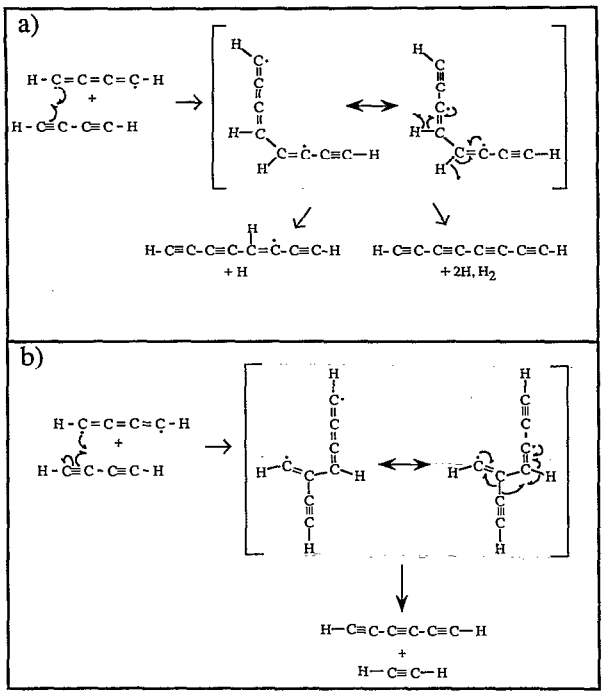

FIG. 11. (a) The proposed mechanism for the formation of both the C_8H_3 and C_8H_2 products from $C_4H_2^*+C_4H_2$. The cumulene-like reactant is the proposed structure for the excited state diacetylene responsible for the observed photochemistry. (b) The proposed mechanism for the formation of $C_6H_2+C_2H_2$.

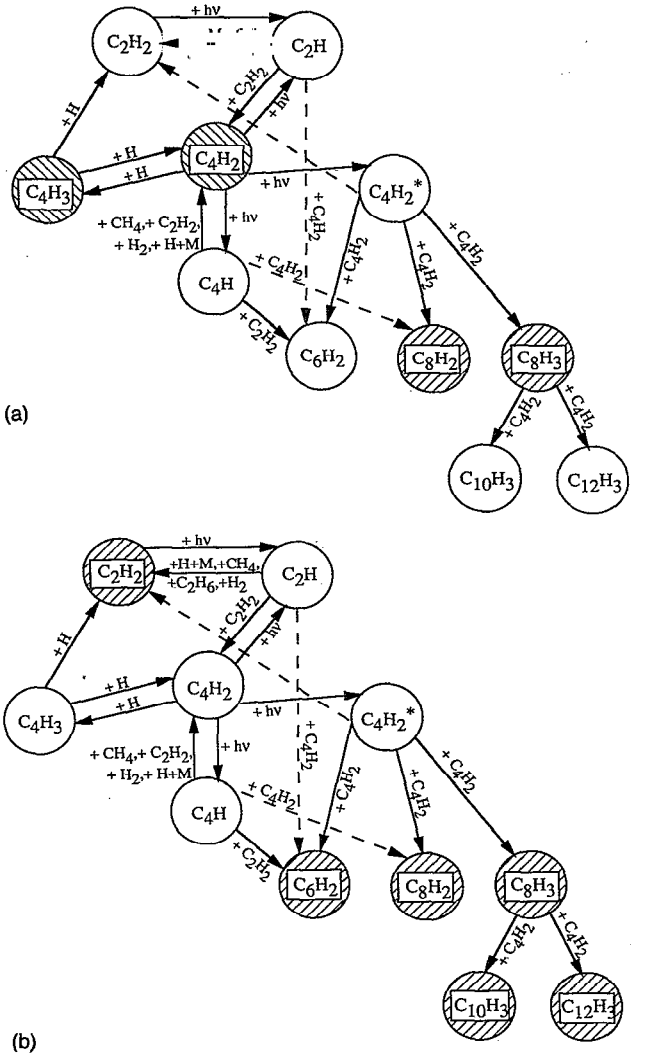

FIG. 12. (a) The photochemical model of hydrocarbon-rich planetary atmospheres involving diacetylene formation and reaction. The double asterisk indicates an excited state molecule. The shaded entries represent modifications to the current model incorporating the products we have observed from the photoexcitation of diacetylene. (b) A second view of the photochemical model which highlights the role of C_4H_2 as a catalyst for recombining free hydrogen atoms (left) and the new source terms for free hydrogen atoms identified in the present study (right).

B. Estimations of photochemical quantum yields

The distribution of products observed in the present study presents an opportunity for determining the absolute photochemical quantum yields for each of the products C_6H_2, C_8H_2, and C_8H_3. It must be recognized that these product quantum yields will depend on the composition and overall pressure of the reaction mixture. This results from the fact that the photochemistry occurs from a metastable excited state in which reaction occurs in competition with deactivation processes within the metastable state which affect the observed product distribution.

The quantum yield for overall loss of C_4H_2 has been reported by Glicker and Okabe as 2.0 ± 0.5 throughout the ultraviolet,[15] indicating that two C_4H_2 molecules react per photon absorbed. We now know that the products formed from this bimolecular reaction are C_6H_2 $(+C_2H_2)$, C_8H_2 $(+2H, H_2)$, and C_8H_3 $(+H)$. In the present experiment, since products are detected following photoionization, the ratio of two product ion intensities is given by

$$\frac{I_{\text{prod}}(1)}{I_{\text{prod}}(2)}=\frac{\phi_{\text{prod}}(1)\sigma_{\text{PI}}(1)f_{\text{det}}(1)}{\phi_{\text{prod}}(2)\sigma_{\text{PI}}(2)f_{\text{det}}(2)},$$

where $\phi_{\text{prod}}(m)$ is the quantum yield for the formation of product m, $\sigma_{\text{PI}}(m)$ is the photoionization cross section of product m at 118 nm, and $f_{\text{det}}(m)$ is the fraction of product m which is transported to the laser interaction volume following formation. Thus the product quantum yields can be determined if the relative photoionization cross sections and detection efficiencies for each of the products are known.

Since the reaction occurs within the quartz reaction tube and close to the ionization source, the differences in detection efficiency are not expected to be great. In addition, the photoionization cross sections for C_6H_2 and C_8H_2 are expected to be similar due to their similar chemical structure. On the other hand, the 118 nm photoionization cross section of C_8H_3 is not known, thwarting the quantitative determination of the product quantum yields. Nevertheless, from the interplay of C_8H_2 and C_8H_3 signals with changing N_2 pressure in the mixture (Fig. 9), it appears that the 118 nm photoionization cross sections for C_8H_2 and C_8H_3 are roughly similar. As a result, a reasonable first

estimate of the photochemical quantum yields for a given reaction mixture follows directly from the relative intensities of the product ions, normalized to a total quantum yield of 2.

C. The $C_4H_2^* + C_4H_2$ reaction in planetary atmospheres

Figure 12(a) depicts a small segment of the current model of methane photochemistry involving diacetylene formation and reaction. This model has been used to predict the composition and aerosol properties of the atmospheres of several planets and satellites.[6] The modifications to the photochemical model involving the primary and secondary products of the $C_4H_2^* + C_4H_2$ reaction are highlighted as shaded entries. As stated earlier, the current photochemical models have postulated that $C_8H_2+H_2$ are the sole initial products of the $C_4H_2^* + C_4H_2$ reaction. The $C_6H_2+C_2H_2$ product channel is denoted by arrows originating from the same point on $C_4H_2^*$ to both C_6H_2 and C_2H_2.

The conditions present in the stratospheres of Titan and the outer planets suggests that ultraviolet absorption by C_4H_2 in these atmospheres will result primarily in metastable $C_4H_2^*$ formation, as occurs in our experiment. As a result, current photochemical models have focused on the $C_4H_2^* + C_4H_2$ reaction as a potentially important route to larger polyynes in the planetary atmospheres. However, since the reaction involves a metastable state, its ultimate importance in planetary atmospheres will depend greatly on the rate of deactivation of $C_4H_2^*$ back to the ground state.[5] Glicker and Okabe's previous work on diacetylene[15] has established that the photochemical quantum yield for diacetylene loss remains 2.0 ± 0.5 even under conditions in which the $(H_2)/(C_4H_2)$ or $(N_2)/(C_4H_2)$ ratios are 1000. Thus, quenching of $C_4H_2^*$ by these major constituents of Titan's atmosphere is inefficient. Nevertheless, quantitative experiments determining the rate constants for quenching of $C_4H_2^*$ are clearly needed since this will allow steady-state $C_4H_2^*$ concentrations to be estimated in the planetary atmospheres.

The present results indicate that the $C_4H_2^* + C_4H_2$ reaction provides a direct route to C_6 and C_8 hydrocarbon products. However, as a minor constituent of the planetary atmospheres, the reaction will occur in competition with $C_4H_2^*$ reactions involving other smaller hydrocarbons including CH_4, C_2H_6, C_2H_2, C_2H_4, and the like. We are currently carrying out experiments to determine the initial products of $C_4H_2^*$ reactions with these molecules. The rate constants for these reactions are also important to obtain.

Finally, the current models of methane photochemistry, most of which originate from the pioneering work of Yung *et al.* on Titan, postulate C_4H_2 as a catalytic route for recombining H atoms from the stratosphere[2]

$$\begin{array}{l} C_4H_2+H+M\rightarrow C_4H_3+M \\ \underline{C_4H_3+H\rightarrow C_4H_2+H_2} \\ \text{Net: } 2H\rightarrow H_2\,. \end{array}$$

These processes are highlighted in Fig. 12(b).

By contrast, the present results indicate that free hydrogen atoms are produced in the reactions

$$C_4H_2^*+C_4H_2\rightarrow C_8H_3+H\rightarrow C_8H_2+2H.$$

Under the N_2-rich conditions similar to those found in Titan's atmosphere, the C_8H_3+H product is the dominant product channel [Fig. 9(c)]. Furthermore, we have shown that much of the C_8H_2 product formed under conditions in which collisional deactivation of $C_4H_2^*$ is inefficient is accompanied by formation of two free hydrogen atoms. Thus, C_4H_2 photochemistry provides unexpected source terms for free hydrogen atoms [Fig. 12(b)], which may partially offset the molecule's role as a catalyst for H-atom recombination.

ACKNOWLEDGMENTS

The authors gratefully acknowledge the National Aeronautics and Space Administration Planetary Atmospheres Program for their support of this work.

[1] D. Gautier and T. Owen, in *Origin and Evolution of Planetary and Satellite Atmospheres*, edited by S. K. Atreya, J. B. Pollack, and M. S. Matthews (University of Arizona, Tucson, 1989), p. 487 ff.
[2] Y. L. Yung, M. Allen, and J. P. Pinto, Astrophys. J. Suppl. Ser. **55**, 465 (1984); Y. L. Yung, Icarus **72**, 468 (1987).
[3] A. Coustenis, B. Bezard, D. Gautier, A. Marten, and R. Samuelson, Icarus **89**, 152 (1991).
[4] P. N. Romani and S. K. Atreya, Icarus **74**, 424 (1988); Geophys. Res. Lett. **16**, 941 (1989).
[5] S. K. Atreya, B. R. Sandel, and P. N. Romani, in *Uranus*, edited by J. T. Bergstralh (University of Arizona, Tucson, 1990); M. E. Summers and D. F. Strobel, Astrophys. J. **346**, 495 (1989).
[6] J. B. Pollack, K. Rages, S. K. Pope, M. G. Tomasko, P. N. Romani, and S. K. Atreya, J. Geophys. Res. **92**, 15037 (1987).
[7] W. R. Thompson, S. K. Singh, B. N. Khare, and C. Sagan, Geophys. Res. Lett. **16**, 981 (1989).
[8] R. A. West, D. F. Strobel, and M. G. Tomasko, Geophys. Res. Lett. **65**, 161 (1986).
[9] E. Karkoschka and M. G. Tomasko, Icarus **97**, 161 (1992); F. Chen, D. L. Judge, C. Y. R. Wu, J. Caldwell, H. P. White, and R. Wagener, J. Geophys. Res. **96**, 17519 (1991).
[10] V. G. Kunde, A. C. Aikin, R. A. Hanel, D. E. Jennings, W. C. Maguire, and R. E. Samuelson, Nature **292**, 686 (1981).
[11] S. J. Harris and A. M. Wiener, Annu. Rev. Phys. Chem. **36**, 31 (1985); R. P. Duran, V. T. Amorebieta, and A. J. Colussi, J. Phys. Chem. **92**, 636 (1988).
[12] K. C. Hou and R. C. Anderson, J. Phys. Chem. **67**, 1579 (1963).
[13] K. Seki, N. Nakashima, N. Nishi, and M. Kinoshita, J. Chem. Phys. **85**, 274 (1986).
[14] G. J. Pontrelli, J. Chem. Phys. **43**, 2571 (1965).
[15] S. Glicker and H. Okabe, J. Phys. Chem. **91**, 437 (1987).
[16] M. Allan, J. Chem. Phys. **80**, 6020 (1984).
[17] R. E. Bandy, C. Lakshminarayan, R. K. Frost, and T. S. Zwier, Science **258**, 1630 (1992).
[18] R. E. Bandy, C. Lakshminarayan, and T. S. Zwier, J. Phys. Chem. **96**, 5337 (1992).
[19] R. J. J. M. Steenvoorden, P. G. Kistemaker, A. E. DeVries, L. Michalak, and N. M. M. Nibbering, Int. J. Mass Spectrom. Ion Proc. **107**, 475 (1991); S. E. Van Bramer and M. V. Johnston, J. Am. Soc. Mass. Spectrom. **1**, 419 (1990); J. Boyle and L. Pfefferle, J. Phys. Chem. **94**, 3336 (1990).
[20] G. Bieri, F. Burger, E. Heilbronner, and J. P. Maier, Helv. Chim. Acta **60**, 2213 (1977).
[21] T. J. Buckley, L. W. Sieck, R. Metz, S. G. Lias, and J. F. Liebman, Int. J. Mass Spectrom. Ion Proc. **65**, 181 (1985).
[22] S. G. Lias, J. E. Bartmess, J. L. Holmes, R. D. Levin, and W. G. Mallard, J. Phys. Chem. Ref. Data **17**, 82 (1988).
[23] The 120 kcal/mol estimate of the C–H bond dissociation energy in

C_4H_2 comes from P. Frank and Th. Just, Combust. Flame **38**, 231 (1980). The C–H bond energy in C_2H_2 has recently been determined at 131.3±0.7 kcal/mol by K. M. Ervin, S. Gronert, S. E. Barlow, M. K. Gilles, A. G. Harrison, V. M. Bierbaum, C. H. DePuy, W. C. Lineberger, and G. B. Ellison, J. Am. Chem. Soc. **112**, 5750 (1990). We take this as an upper bound for the bond strength in C_4H_2.

[24] A. Karpfen and H. Lischka, Chem. Phys. **102**, 91 (1986).

[25] A. Fahr and A. H. Laufer, J. Phys. Chem. **90**, 5064 (1986).